

CP Violation Prospects at the LHC

H. B. Dijkstra

CERN, CH-1211 Geneva 23, Switzerland

Received on 5 January, 2004

In the last few years experiments at B-factories have established CP violation in B_d decays. From 2007 onward new experiments will start to exploit the large $b\bar{b}$ cross-section at the LHC to advance the understanding of CP violation by studying unprecedented large samples of all B-meson flavours. After a short review of the present status, the experimental challenges for the future experiments will be described. The emphasis will be on LHCb, a dedicated B-physics experiment at the LHC, and some examples of the projected physics results will be presented.

1 Introduction

In the Standard Model the charged current interactions of quarks is described by the Cabibbo-Kobayashi-Maskawa (CKM) matrix [1], i.e. the matrix gives the couplings of W^+ -boson between the three families of up-down quark pairs:

$$V = \begin{pmatrix} V_{ud} & V_{us} & V_{ub} \\ V_{cd} & V_{cs} & V_{cb} \\ V_{td} & V_{ts} & V_{tb} \end{pmatrix}.$$

Since it is unitary, the matrix can be parametrised with four independent parameters, including one phase, which introduces CP violation. One of the commonly used parameterisations, introduced by Wolfenstein [2], is based on the parameters: λ , A , ρ and η . In this parametrisation, V can be approximated as

$$V \approx \begin{pmatrix} 1 - \lambda^2/2 & \lambda & A\lambda^3(\rho - i\eta) \\ -\lambda & 1 - \lambda^2/2 & A\lambda^2 \\ A\lambda^3(1 - \rho - i\eta) & -A\lambda^2 & 1 \end{pmatrix},$$

where $\lambda = \sin(\theta_{\text{Cabibbo}}) = 0.2240 \pm 0.0036$ [3], and only terms up to λ^3 are included.

The first observation of CP violation was in the neutral kaon system, and dates back to 1964. This phenomenon in combination with the work of Kobayashi and Maskawa led to the prediction of a third quark generation. The measurement of CP violation could lead eventually to the precise determination, and even over-constraint, of the CKM matrix elements if they can all consistently be described in the Standard Model framework. However, the hope is that new physics beyond the Standard Model will show up in a detailed comparison of the CP violating observables of many decays. The rationale behind this expectation is that many extensions of the Standard Model introduce additional sources of CP violation, which modify CP observables in a way that they can be distinguished from the Standard Model mechanism [4]. It cannot be excluded that new physics at mass scales beyond the reach of direct searches will produce measurable effects in the CP violation sector. Another reason

for the expectation that new physics beyond the Standard Model might manifest itself via CP violation is that it is one of the three conditions for baryogenesis [5]. However, the CP violation generated through the CKM-phase appears to be far too small to generate the observed imbalance between matter and anti-matter in our universe.

Among the nine unitarity relation of the CKM matrix the following is one of the most relevant for B-hadron decays:

$$V_{ud}V_{ub}^* + V_{cd}V_{cb}^* + V_{td}V_{tb}^* = 0$$

A pictorial way to represent the above relation in the modified Wolfenstein parameters $[\rho, \eta]$ plane, which include a higher order correction in λ , is shown in Fig. 1. The angles denoted in the triangles are defined as: $\alpha = \arg(-\frac{V_{td}V_{tb}^*}{V_{ud}V_{ub}^*})$, $\beta = \arg(-\frac{V_{cd}V_{cb}^*}{V_{td}V_{tb}^*})$ and $\gamma = \arg(-\frac{V_{ud}V_{ub}^*}{V_{cd}V_{cb}^*})$, and these angles can be accessed with CP violation measurements in B-decays.

2 CP Violation at the B-factories

The constraints on the CKM matrix [6] from all available measurements in the summer of 2003, but excluding the CP violation measurements in B-decays is shown in Fig. 2. The constraints come from $|V_{ub}/V_{cb}|$, which is measured from tree diagram B-decays, from ϵ_K , the CP violation in the neutral kaon system, and from Δm_d and the lower limit on Δm_s . It should be noted that Δm_d is measured with high precision, but its interpretation in the CKM matrix is dominated by theoretical uncertainties. The result of the Standard Model fit [3] gives $0.646 < \sin(2\beta) < 0.789$ with a 95% confidence level.

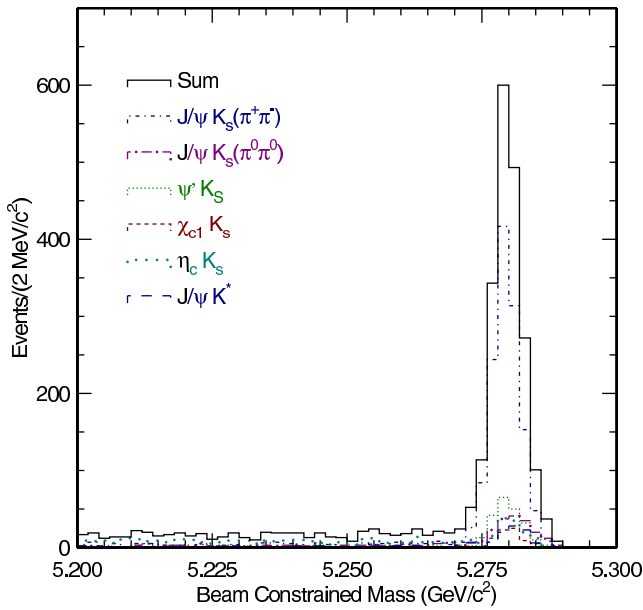


Figure 5. Beam constrained mass of the various $b \rightarrow c$ transitions used by Belle to extract the asymmetry.

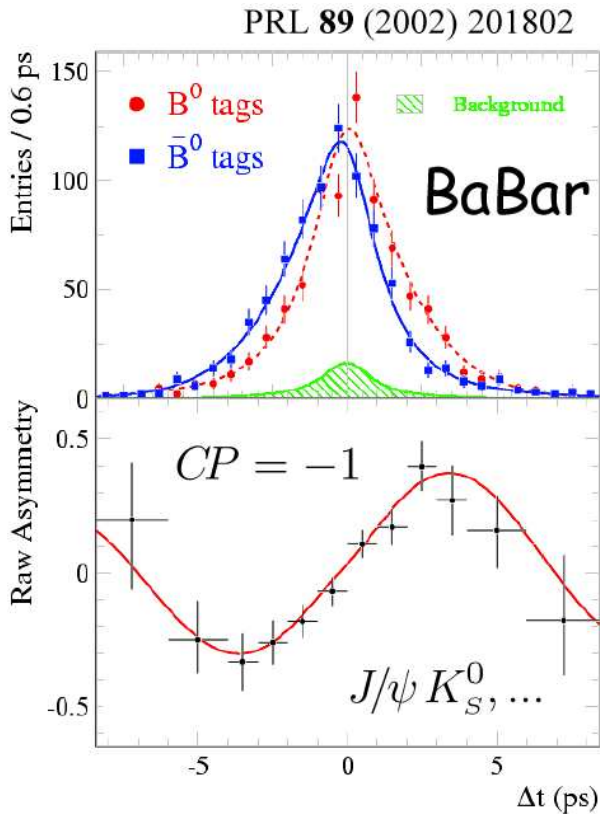


Figure 6. The raw asymmetry in various $b \rightarrow c$ transitions as measured by BaBar.

duction, is measured as a function of Δt , and fitted with the expression $A^{\text{dir}} \cos(\Delta m \Delta t) + A^{\text{mix}} \sin(\Delta m \Delta t)$. The Standard Model expectations are $A^{\text{dir}} = 0$, and $A^{\text{mix}} = \sin(2\beta)$. Fig. 5 shows the beam constrained mass ($\sqrt{(E_{\text{CM}}/2)^2 - (\vec{p}_{J/\psi} + \vec{p}_{K_S})^2}$) of the various $b \rightarrow c$ transitions used by Belle to extract the asymmetry. Fig. 6 shows

the raw asymmetry as measured by Babar [10], and the result of the unbinned likelihood fit to extract the asymmetry parameters.

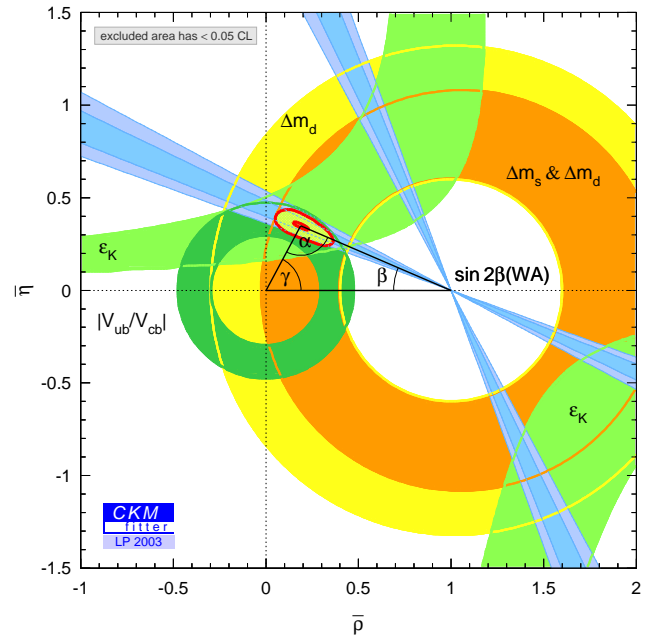


Figure 7. Confidence levels in the $[\bar{\rho}, \bar{\eta}]$ plane as obtained by the CKMfitter group, including information from CP violation measurements in charmonium B-decays.

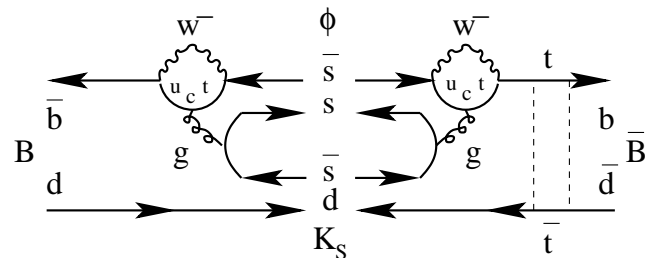


Figure 8. Penguin diagram for generating $B_d \rightarrow \phi K_S^0$ decays.

Assuming that only Standard Model box diagrams contribute to the $B - \bar{B}$ mixing, the collaborations have measured for $\sin(2\beta)$:

$$\begin{aligned} \text{Belle: } & 0.719 \pm 0.074(\text{stat}) \pm 0.035(\text{syst}) \\ \text{Babar: } & 0.741 \pm 0.067(\text{stat}) \pm 0.034(\text{syst}) \end{aligned}$$

In excellent agreement with the prediction from a combined fit of the CKM elements presented above. Fig. 7 shows the constraints on the CKM matrix [6] from all available measurements in the summer of 2003, including the CP violation measurements in the charmonium B-decays. Hence, the Kobayashi-Maskawa mechanism can explain CP violation in flavour changing processes. In addition, the first measurements of CP violation in the B-system imposes a significant constraint. However, this does not excluded new physics contributions. The decay $B_d \rightarrow \phi(\rightarrow K^+K^-)K_S^0(\rightarrow \pi^+\pi^-)$, cannot proceed via a tree diagram, since it is a transition of $bd \rightarrow sssd$ quarks, hence only involving down quarks. A corresponding Feynman diagram for the Standard

Model penguin process is shown in Fig. 8, and since the penguin loop with the top quark dominates, CP violation in the decay can be neglected, and so for ϕK_S the CP violation is expected to be dominated by the interference of decays with and without mixing. Hence in the Standard Model it is expected that $\sin(2\beta)_{\phi K_S} \approx \sin(2\beta)_{\phi K_S^0}$. The two measurements are expected to agree within $\mathcal{O}(\lambda^\epsilon)$ [11], or a few %. But new (s)particles in the penguin loop could modify this, making the discrepancy $\mathcal{O}(\lambda)$ or even $\mathcal{O}(\infty)$. Experimentally these penguin decays are much more challenging, with the $\text{BR}(B_d \rightarrow \phi(\rightarrow K^+K^-)K_S^0(\rightarrow \pi^+\pi^-)) = 1.4 \times 10^{-6}$. Both Belle and Babar have reconstructed about 70 events consistent with the decay $B_d \rightarrow \phi K_S^0$. At the 2003 summer conferences they reported [12] based on a total of 250 fb^{-1} for $\sin(2\beta)_{\phi K_S}$:

$$\begin{aligned} \text{Belle: } & -0.96 \pm 0.50(\text{stat})_{-0.11}^{+0.09}(\text{syst}) \\ \text{Babar: } & +0.45 \pm 0.43(\text{stat}) \pm 0.07(\text{syst}) \end{aligned}$$

Fig. 9 summarizes the measurements of $\sin(2\beta_{\text{eff}})$ of both the charmonium and s-penguin decays of the B_d . The results show a tendency of $\sin(2\beta_{\text{eff}})$ of s-penguin decays to deviate from the determination of $\sin(2\beta)$ from tree processes by more than what is expected within the Standard Model. However, the deviation is still not statistically significant. By 2006 it is expected that the data volume at the B-factories has increased from 250 fb^{-1} now to 1000 fb^{-1} .

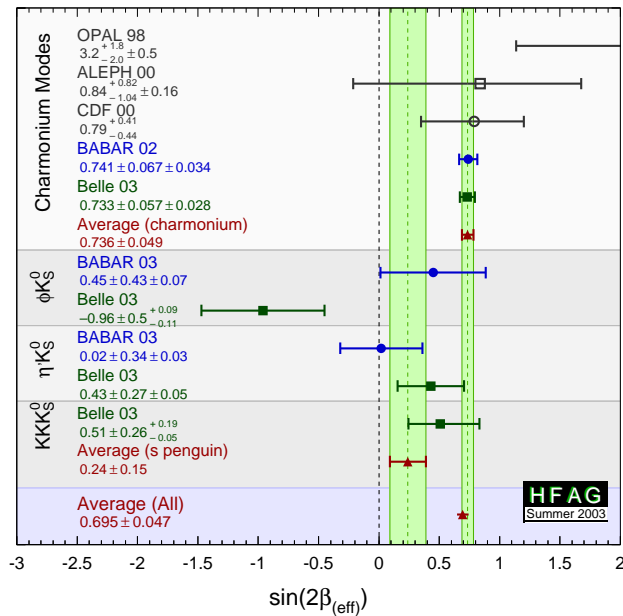


Figure 9. Summary of the measurements of $\sin(2\beta_{\text{eff}})$ as made by [13].

Up till now CP violation in the B-system has only been firmly established in the $b \rightarrow c\bar{c}s$ CP-eigenstates. Apart from looking for signs of new physics in comparing tree and penguin decays as presented above, other fruitful ways to check deviations from the Standard Model are to compare the other CKM-angles, and in particular the check: $\alpha + \beta + \gamma = \pi$. As an example α can be accessed at B-factories by measuring a charmless CP-eigenstate like $B_d \rightarrow \pi^+\pi^-$. Table II shows the asymmetries measured by

Belle [14] and BaBar [15] in $B_d \rightarrow \pi^+\pi^-$ decays. This particular decay has both tree and penguin contributions, and interpreting measured asymmetries within the Standard Model in terms of constraints on the CKM matrix parameters without having to rely on model dependent theoretical inputs would require integrated luminosities at the B-factories of order 10 ab^{-1} [16]. This is an order of magnitude larger than what is foreseen to be accumulated before the start of the LHC in 2007.

TABLE II. The asymmetries measured for the decay $B_d \rightarrow \pi^+\pi^-$.

	Babar	Belle
$\int L$	113 fb^{-1}	78 fb^{-1}
A^{mix}	$-0.40 \pm 0.22 \pm 0.03$	$-1.23 \pm 0.41_{-0.07}^{+0.08}$
A^{dir}	$0.19 \pm 0.19 \pm 0.05$	$0.77 \pm 0.27 \pm 0.08$

3 $b\bar{b}$ -production at the LHC

The Large Hadron Collider (LHC) at CERN will collide protons at a center of mass energy of 14 TeV. The processes which dominate the production of $b\bar{b}$ -pairs can be subdivided in three categories: flavour creation, flavour excitation and fragmentation. Flavour creation proceeds via two to two parton processes of the type $q+\bar{q} \rightarrow b+\bar{b}$ and $g+g \rightarrow b+\bar{b}$, i.e. the annihilation of light quarks or the fusion of gluons. In flavour excitation a (\bar{b})-quark from the sea of one proton scatters with a parton from the other proton, making it very sensitive to the structure functions which describe the $b\bar{b}$ content of the proton. The fragmentation category contains processes where the b-quarks do not participate in the initial hard parton scattering process, but where $b\bar{b}$ -pairs are produced via f.i. gluon splitting. The relative contributions of the three categories have been studied at the Tevatron [17] by comparing inclusive b-quark cross-sections with Monte-Carlo models. Fig. 10 shows CDF and D0 data on the integrated inclusive b-quark total cross-section for $p_T > p_T^{\text{min}}$ in $p\bar{p}$ collisions at $\sqrt{s} = 1.8 \text{ TeV}$. The data is compared with PYTHIA 6.158 [18] using the CTEQ4L structure functions. The Monte-Carlo model contributions are split in the three categories discussed above.

To model the $b\bar{b}$ -production at $\sqrt{s} = 14 \text{ TeV}$ PYTHIA parameters have been tuned to data at lower energies, and the corresponding parameters have been extrapolated to the LHC energy. The LHCb collaboration [19] uses PYTHIA 6.2 with the CTEQ4L structure functions, and charged multiplicity distributions from CDF and UA5 to make this extrapolation [20], and obtains that PYTHIA predicts a total inelastic cross section of 79.2 mb, and a $b\bar{b}$ production cross section of $633 \mu\text{b}$.

The experiments at the LHC which will exploit the large $b\bar{b}$ production cross section are two central detectors (ATLAS and CMS) and one forward spectrometer (LHCb), and will be introduced in more detail in the next section. For most CP measurements it is necessary to tag the flavour of the b-quark before it mixes, and hence the experiments have

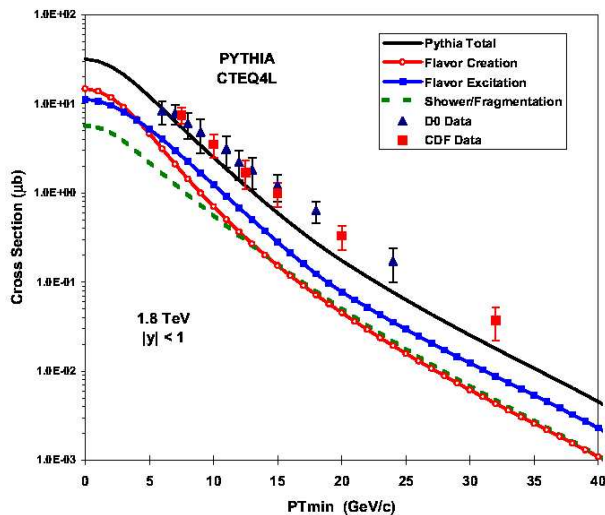


Figure 10. Total b-inclusive cross-section at $\sqrt{s} = 1.8$ TeV as measured by CDF and D0 in the central rapidity region $|y| < 1$, and compared to the expectation from PYTHIA 6.158 split out in the different processes discussed in the text.

to detect decay products of both b-quarks in the same event. Fig. 11 shows the expected correlation between the two b-quarks in pseudo-rapidity at 14 TeV, and overlaid the acceptances of a central detector (ATLAS) and a forward spectrometer (LHCb). The only data available on b-production is in the central region, while LHCb will operate at much large values of the pseudo-rapidity range. In addition, the correlation between the b-quarks depends on the production process, hence increasing the uncertainty in the expected number of reconstructed and tagged B-events. For the estimated event yields at the LHC it is therefore conservatively assumed that the total $b\bar{b}$ cross-section is $500 \mu\text{b}$, rather than the $633 \mu\text{b}$ predicted by PYTHIA.

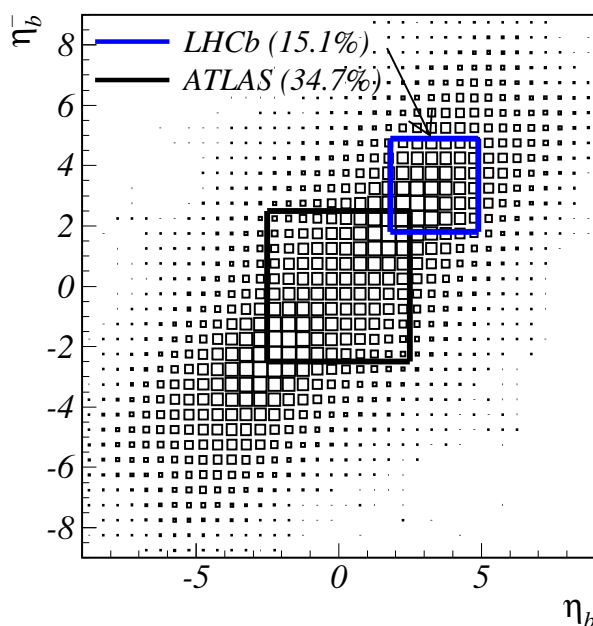


Figure 11. The correlation between the pseudo-rapidities (η) of the two b-quarks as expected by PYTHIA in pp-interactions at 14 TeV. The acceptance of LHCb and ATLAS at the LHC are overlaid.

Apart from a copious production of B^0 and B^\pm , it is expected that of all B-hadrons produced at the LHC, about 12% will be B_s , and about 10% will be beauty baryons. The design luminosity of the LHC machine is foreseen to be $1 - 2 \times 10^{33} \text{ cm}^{-2}\text{s}^{-1}$ at the start-up, and after a several years $10^{34} \text{ cm}^{-2}\text{s}^{-1}$. LHCb has chosen to run around $2 \times 10^{32} \text{ cm}^{-2}\text{s}^{-1}$, to facilitate the triggering and reconstruction, and to make the radiation damage in the forward region more manageable. Even at this lower luminosity, the number of $b\bar{b}$ -pairs produced at the LHC per unit time exceed the production at a B-factory by four orders of magnitude. However, apart from these advantages, compared to the B-factories the $\sigma(b\bar{b})/\sigma(\text{inelastic})$ at the LHC is 30 times larger. This, combined with the large luminosity, creates a challenging experimental environment. The detectors are subject to radiation damage, and the charged track multiplicity per pp-interaction is typically about 30 within the acceptance of LHCb ($1.8 < \eta < 4.9$) in events which contain a $b\bar{b}$ -pair. In addition the tagging at LHC is more diluted compared to the B-factories, since the b-quarks do not evolve coherently, and the tagging B-meson might even be a rapidly oscillating B_s .

4 LHC B-physics Experiments Overview

At the LHC there are three detectors in which CP violation in the B-system is included in their scientific program: ATLAS [21], CMS [22] and LHCb [19]. ATLAS (Fig. 12) and CMS (Fig. 13) are both central detectors, covering $-2.5 < \eta < 2.5$ in pseudo-rapidity and optimised for direct searches of Higgs and supersymmetry. Both experiments are equipped with full Silicon tracking systems inside a solenoidal magnetic field, which allows the reconstruction of B-decay products and measure its proper time. Their first level triggers are aimed at reducing the 40 MHz LHC frequency to 50-100 kHz using a combination of muon and jet triggers from the calorimeters and muon chambers. Their B-physics program relies on being able to set thresholds for muons low enough to be sensitive to B-decays, while keeping the rate of these trigger low compared to triggers aimed at the searches for new particles. Typically a p_T threshold of 6-7 GeV/c is planned for during the first years of LHC operation at relatively low luminosities. Hence, this trigger selects only B-mesons which are produced with a relatively large p_T , hence reducing its efficiency as can be seen in Fig. 10. When LHC reaches its design luminosity, the thresholds would have to be set too high to remain sensitive to B-physics. The muon triggers address especially B-decays which involve ψ mesons, while hadronic B-decays are selected by triggering on the semi-leptonic decay of the tagging B in the first level trigger, and attempting to reconstruct the hadronic decay in higher level triggers in addition. The experiments have very limited π/K separation capability, which makes them only competitive in channels where particle identification is not crucial.

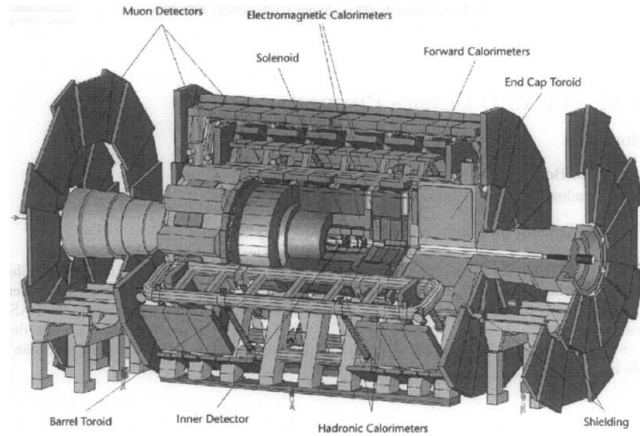


Figure 12. The ATLAS detector, showing.

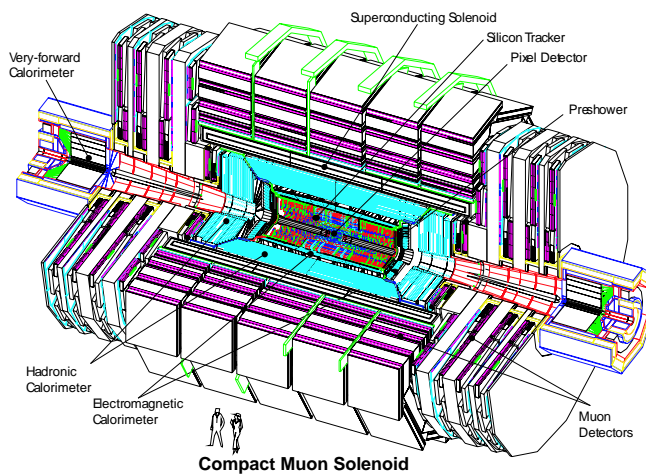


Figure 13. The CMS detector.

LHCb is a dedicated experiment for making precise studies of CP asymmetries and rare decays in the b-hadron system, and its spectrometer is shown in Fig. 14.

It is a single arm spectrometer covering the range $1.9 < \eta < 4.9$. It consists of a Silicon Vertex Locator (VELO) and four Silicon Trigger Tracker (TT) planes before a 4 Tm di-pole magnet. The tracking system behind the magnet consists of three multi-layer chambers (T1-T3), each chamber consisting of three of four Silicon planes close to the beam-line, surrounded by eight layers of 5 mm diameter straw tubes. Two Ring Imaging Cherenkov detectors (RICH1&2) provide π/K separation over the momentum interval $2 < p < 100$ GeV/c. The calorimeter system consists of a Scintillating Pad Detector (SPD) to distinguish charged particles from photons, a Pre-Shower (PS), an Electromagnetic Calorimeter (ECAL) based on the Shashlik type, and a Hadronic Calorimeter (HCAL). Behind the calorimeter four Muon Chambers (M2-M5) provide muon reconstruction and identification capability, while M1 is used to improve the momentum resolution in the first trigger level. The low- β insertion at the LHCb interaction point allows LHCb to run at luminosities between $2 - 5 \times 10^{32} \text{ cm}^{-2}\text{s}^{-1}$, even when the

LHC reaches its design luminosity of $10^{34} \text{ cm}^{-2}\text{s}^{-1}$. LHCb aims at running at these relatively low luminosities to avoid too much pile-up, note that at $10^{34} \text{ cm}^{-2}\text{s}^{-1}$ there are about 20 pp-interaction per crossing, while at $2 \times 10^{32} \text{ cm}^{-2}\text{s}^{-1}$ 80% of the crossings with interactions have only one visible interaction. Fig. 15 shows a typical B-event in LHCb. Note that most of the low momentum secondaries are trapped in the magnetic field inside the magnet, where no sensitive elements are placed. On average LHCb reconstructs 26 tracks with hits in both the VELO and T1-T3.

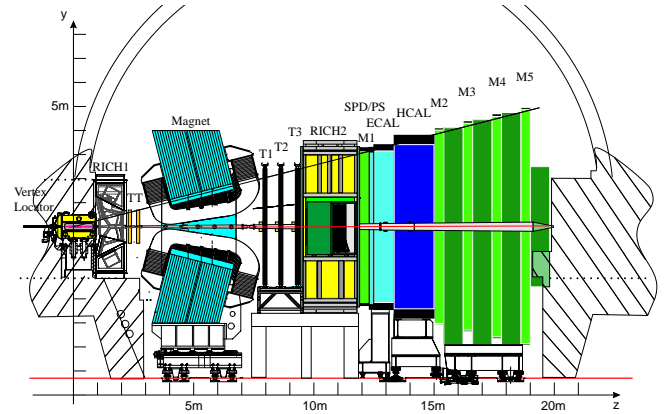


Figure 14. The LHCb detector, showing the VELO, TT and T1-3 tracking elements. The 4 Tm di-pole magnet, RICH1&2, the calorimeter system and the muon chambers.

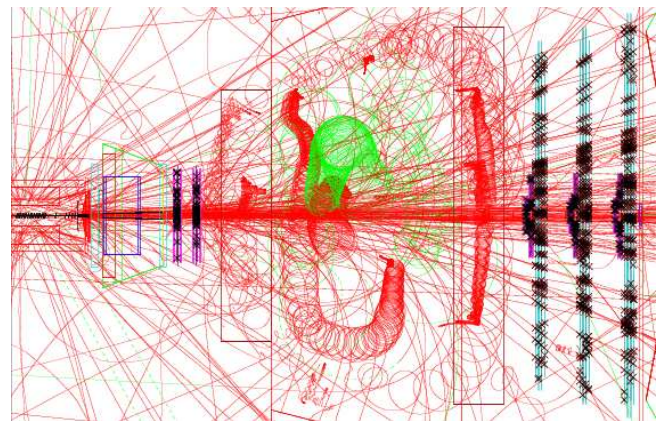


Figure 15. The typical event in LHCb as produced by GEANT3.

What sets LHCb apart from the general purpose detectors ATLAS and CMS is especially the VELO, its trigger scheme, and the RICH detectors, and these will be presented in some more detail in the next sections.

5 Vertex Detection

To detect the B-decay products, reconstruct the primary vertex and measure the proper time of the B-mesons all three experiments utilize Silicon sensors close to the interaction region. The CMS tracking system [23] encompassed a total of 210 m^2 of Silicon strip sensors, read-out via 10^7 channels. The core of the tracking system consists of Silicon

pixel detectors (see Fig. 16), arranged in three barrels with $44 < radius < 102$ mm and end-caps. The size of the $45 \cdot 10^6$ pixels is $150 \times 150 \mu\text{m}^2$, which, using charge division, provides a resolution of about $12 \mu\text{m}$ in $r\phi$. The ATLAS tracking system [24] consist of 65 m^2 of Silicon strip sensors, read-out with 6×10^6 channels. Like CMS, ATLAS has chosen to cope with the large track density and high radion damage close to the interaction point with a system of pixel detectors, as is shown in Fig. 17. It consist of three barrel layers between 5-13 cm radius, which contain 80×10^6 pixels of $50 \times 300 \mu\text{m}^2$, complemented with end-caps. The binary read-out provides about $12 \mu\text{m}$ resolution in $r\phi$.

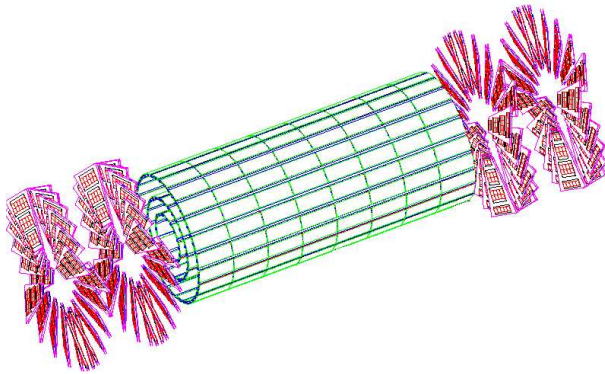


Figure 16. Schematic of the CMS pixel detector.

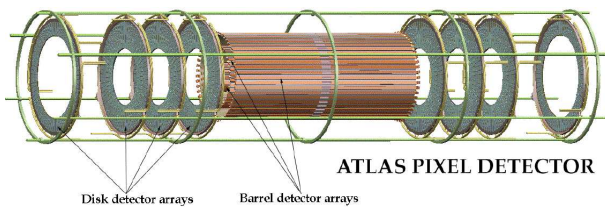


Figure 17. Schematic of the ATLAS pixel detector.

The forward geometry of LHCb is covered close to the interaction region with 0.23 m^2 of Silicon strip detectors [25], read-out by 170k channels. There are two types of sensors, sensors with strips at constant radius (R-sensors), and sensors with quasi radial strips (Φ -sensors). An R- and Φ -sensor form one half-station, and the 42 half-stations are arranged perpendicular to the beam-line as is shown in Fig. 18. The strip pitch and length varies as a function of the radial position of the strips, with strips close to the beam-line having a pitch of $40 \mu\text{m}$ and being only 6 mm long. Using charge division a resolution down to $7 \mu\text{m}$ is obtained. The sensitive area of the sensors starts at only 8 mm from the beam-line, resulting in a radiation dose several times larger than what is expected in ATLAS and CMS, despite the much reduced luminosity. It is foreseen to replace the sensors every few years. The aperture required by the LHC beam during injection requires the sensors to be retracted to a distance of 3 cm from the beam line, and hence the sensors are placed

in Roman-pots, and are separated from the LHC vacuum by a $250 \mu\text{m}$ thick Al-foil.

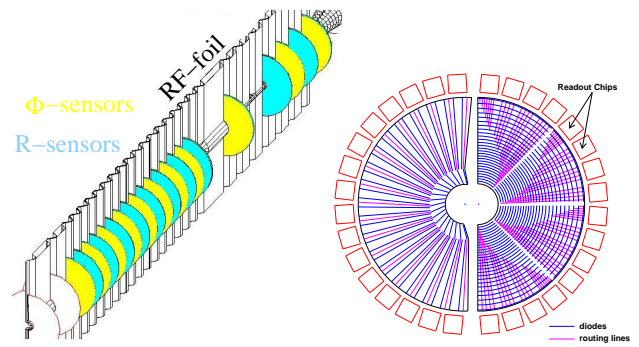


Figure 18. Schematic of the LHCb VELO.

Excellent proper time resolution is not only required to distinguish B-meson decays from a large combinatoric background, but is also essential to resolve the fast oscillation of B_s mesons, which is expected to be $\Delta m_s = 18.3 \pm 1.7 \text{ ps}^{-1}$ [3]. The value of Δm_s can be measured in $B_s \rightarrow D_s^- \pi^+$ decays, and the proper time resolution expected for this decay in ATLAS, CMS and LHCb is 70 ps^{-1} , 65 ps^{-1} and 40 ps^{-1} respectively. Fig. 19 shows the proper time distribution of $B_s \rightarrow D_s^- \pi^+$ candidates as simulated and reconstructed by LHCb for two different assumptions of Δm_s . Based on one year of data LHCb is expected to be able to make a five standard deviation observation of B_s oscillation up to $\Delta m_s = 68 \text{ ps}^{-1}$ [19]. If Δm_s turns out to be close to its the Standard Model expectation, LHCb should be able to measure it within a few weeks of running. The corresponding reach for the equivalent of one year of ATLAS [26], i.e. 10 fb^{-1} , is 22.5 ps^{-1} . The difference in reach is not only driven by the superior impact parameter resolution of LHCb, but also by the much larger statistics which can be accumulated by LHCb for this channel due to its trigger, which will be described in the next section.

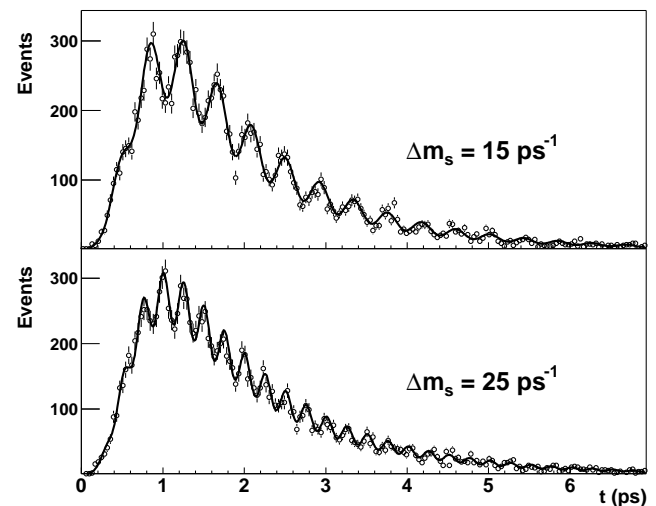


Figure 19. Proper time distribution of $B_s \rightarrow D_s^- \pi^+$ candidates corresponding to one year of LHCb operation. Only those events are shown which have been tagged as having not oscillated.

6 Triggering on B-mesons

Table III gives an overview of the different strategies utilised by the three experiments to reduce the LHC 40 MHz clock frequency to the few hundred Hz of events which will be written to storage.

Both ATLAS [27] and CMS [28] use the first hardware based trigger level to reduce the rate to <100 kHz, by requiring a muon or two muons to be present with sufficient p_T . The actual p_T thresholds which will be applied for the B-physics trigger will depend on the available band-width for these triggers at the different luminosities. Thresholds which still give a competitive efficiency in the range 4-14 GeV/c for the single muon trigger can only be employed for low luminosities around $10^{33} \text{ cm}^{-2}\text{s}^{-1}$ during the start-up phase of the LHC, or maybe at the end of a fill. Based on the hardware trigger ATLAS defines Regions-of-Interest (RoI), and the data inside a RoI is transferred to a CPU for further selection. Full event building is then performed at a rate of 1 kHz, after which High Level Trigger (HLT) algorithms make the final selection to reduce the rate to 100 Hz. CMS performs full event building already at a rate of 100 kHz, which is reduced at start-up to 50 kHz. Their HLT first performs a pre-HLT, based on the information from the hardware trigger, to reduce the rate at which full track reconstruction can be performed for the final selection of the about 100 Hz of events written to storage.

TABLE III. Overview of trigger strategies of ATLAS, CMS and LHCb for triggering on B-mesons.

	ATLAS	CMS	LHCb
Rate	40 MHz	40 MHz	40 MHz
Data	$\mu, \mu\mu$	$\mu, \mu\mu$	$\mu, \mu\mu, e, \gamma, \pi^0, h$
Type	Hardware	Hardware	Hardware
Rate			1 MHz
Data			VELO, TT, first level objects
Type			CPU-farm
Rate	70 – 100 kHz	< 100 kHz	40 kHz
Data	RoI	Full event	Full event
Type	CPU-farm	CPU-farm	CPU-farm
Algorithm	Seed based	Seed based	Seed based
Rate	1 kHz	variable	< 20 kHz
Data	Full event	Full event	Full event
Type	CPU-farm	CPU-farm	CPU-farm
Storage	100 Hz	100 Hz	200 Hz

The LHCb [29] trigger is dedicated to select B-mesons, and hence aims at being able to trigger on relatively small p_T hadrons, leptons or photons with high efficiency. Fig. 20 shows a schematic of the LHCb trigger system. The LHCb trigger is subdivided in three trigger levels, called Level-0, Level-1 and HLT. The LHC beam crossing rate of 40 MHz contains about 10 MHz of crossings with visible pp-interactions at the LHCb luminosity, and the hardware trigger is used to reduce this rate to a rate at which in principle all sub-systems could be used for deriving a trigger decision.

Due to a combination of their large mass and p_T b-hadrons decay to give a large E_T lepton, hadron or photon. Level-0 reconstructs:

- the highest E_T hadron, electron and photon clusters in the Calorimeter,
- up to the two highest p_T muons in the Muon Chambers,

which information is collected by the Level-0 Decision Unit to select events. Events can be rejected based on global event variables such as charged track multiplicities and the number of interactions, as reconstructed by the Pile-Up system, to assure that the selection is based on b-signatures rather than large combinatorics, and that these events will not occupy a disproportional fraction of the data-flow bandwidth or available processing power in subsequent trigger levels.

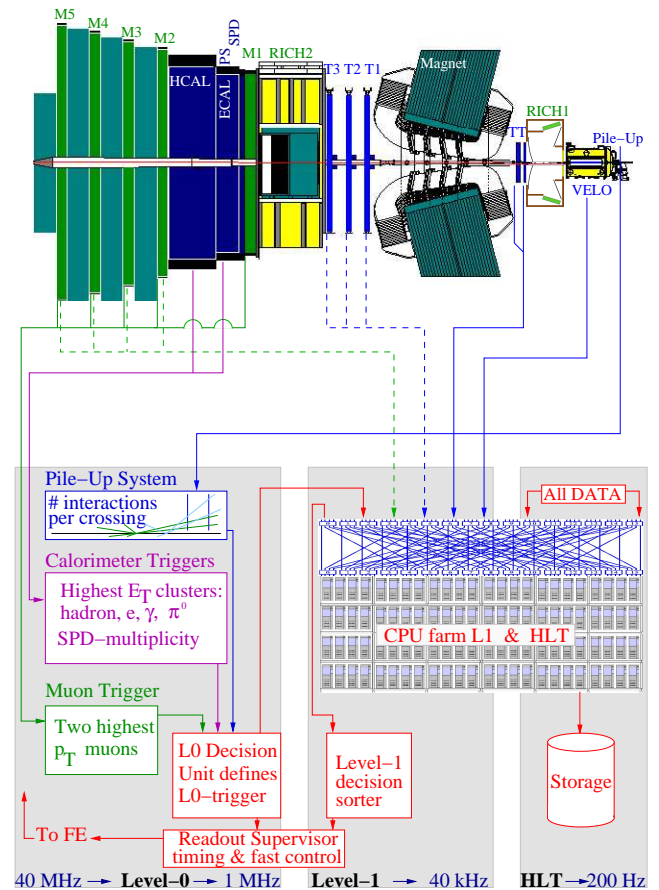


Figure 20. Schematic of the LHCb Trigger System.

The implementation of the calorimeter trigger is based on forming clusters by adding the E_T of 2×2 cells on the FE-boards, and selecting the clusters with the largest E_T . Clusters are identified as e, γ or hadron depending on the information from the SPD, PS, ECAL and HCAL. The E_T of all HCAL cells is summed to reject crossings without visible interactions. The total number of SPD cells with a hit

are counted to provide a measure of the charged track multiplicity in the crossing.

The muon chambers allow stand-alone muon reconstruction with a p_T resolution of 20%. Track finding is performed in the five muon stations by combining the strips and pads to form towers pointing towards the interaction region, and the two muons with the largest p_T in the crossing are reconstructed.

The Pile-Up system aims at distinguishing between crossings with single and multiple visible interactions. It uses four R-sensors of the same type as those used in the VELO to measure the radial position of tracks, covering $-4.2 < \eta < -2.9$. The Pile-Up system provides the position of the primary vertex candidates along the beam-line and a measure of the total backward charged track multiplicity.

The Level-0 Decision Unit (LODU) collects all information from Level-0, and with simple arithmetic combines all signatures into one decision per crossing.

At the 1 MHz output rate of Level-0 the remaining analogue data is digitized and all data is stored for the time needed to process the Level-1 algorithm. The Level-1 algorithm will be implemented on a commodity processors farm, which is shared between Level-1, HLT and offline reconstruction algorithms. The Level-1 algorithm uses the information from Level-0, the VELO and TT. The algorithm reconstructs tracks in the VELO, and matches these tracks to Level-0 muons or Calorimeter clusters to identify them and measure their momenta. The fringe field of the magnet between the VELO and TT is used to determine the momenta of particles with a resolution of 20–40%. Events are selected based on tracks with a large p_T and significant impact parameter to the primary vertex. Fig. 21 shows the sum of $\log(p_T)$ of the tracks with the largest p_T in the event, and the sum of $\log(d/\sigma_d)$, their impact parameter significance, as determined by the Level-1 algorithm. The maximum Level-1 output rate has been fixed to 40 kHz, at which rate full event building is performed. The implementation is easily scalable to allow the inclusion of stations T1–T3 and M2–M5, which will improve the Level-1 performance.

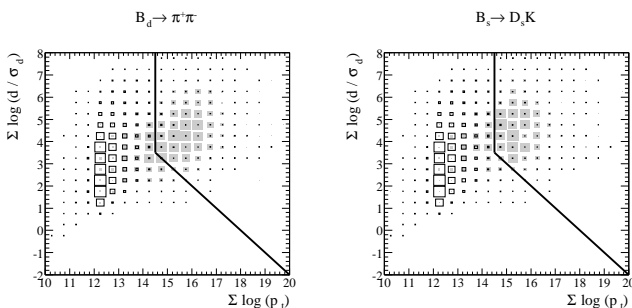


Figure 21. Distributon of off-line selected signal events (closed squares) and minimum bias events (open squares) in the plane of the two discriminating variables used by the LHCb Level-1 trigger.

The HLT will have access to all data. Level-1 and HLT event building share the same network. The HLT and Level-1 algorithms run concurrently on the same CPU nodes, with the Level-1 taking priority due to its limited latency budget of 58 ms. The HLT algorithm starts with a pre-trigger, which

aims at confirming the Level-1 decision with better resolution, followed by selection algorithms dedicated to either select specific final states, or generic cuts to enrich the B-content of the events written to storage. The total CPU farm will contain about 1800 nodes, and the L1 and HLT algorithms will use about 55% and 25% of the available computing resources respectively. The remaining resources are used to fully reconstruct events accepted by the HLT, including the particle identification, before being written to storage. Fig. 22 shows the efficiency achieved by LHCb for some representative channels by the Level-0 and Level-1 triggers, measured for events which pass the off-line selection cuts, which have been tuned to achieve sufficient background rejection. It is expected that the HLT trigger will reach nearly 100% efficiency. Fig. 23 shows the expected annual un-tagged event rates after trigger and off-line selection cuts.

The expected yield for 10 fb^{-1} by ATLAS and CMS for $B_s \rightarrow \psi(\rightarrow \mu^+ \mu^-) \phi(\rightarrow K^+ K^-)$, a channel which is favoured by the first level trigger, is 100k and 84k events respectively. The corresponding annual event yield of LHCb is 100k events. For channels which do not contain muons the LHCb trigger provides a large advantage, since it can also trigger on hadronic final states. ATLAS and CMS can only trigger these events in their first trigger levels via a semi-leptonic decay of the tagging B-meson in a muon. ATLAS and CMS expect for $B_s \rightarrow D_s^-(\rightarrow K^+ K^- \pi^-) \pi^+$ a yield of 3.3k and 0.15-5.5k events respectively. The large range of the yield of CMS reflects the range in threshold settings of the first level trigger, which will depend on the allowed bandwidth for B-physics. The corresponding annual yield in LHCb is 80k events, however the ATLAS and CMS events will nearly all be tagged because of the first level trigger selection on the muon. The correspondin tagged LHCb yield will be 44k events, still an order of magnitude larger.

At one of the B-factories the yield in $B_d \rightarrow \psi(\rightarrow \mu^+ \mu^-) K_S^0$ so far is about 2k events. The corresponding annual yield expected in LHCb will be 220k events. Similarly the expected rate for $B_s \rightarrow \pi^+ \pi^-$ at a B-factory so far is 200 events, while LHCb expects 26k events per year. Hence due to trigger and acceptance losses the four orders larger $b\bar{b}$ production in LHCb has been reduced to about two orders of magnitude of useful events. For final states which require tagging, the B-factories have the advantage that the B-mesons evolve coherently, and that there is no spectator background in the event. As a consequence the effective tagging efficiency $\epsilon_{eff} = \epsilon_{tag}(1 - 2w)^2$, where ϵ_{tag} is the efficiency to tag an event and w is the mis-tag probability, at the B-factories is 28%, while in LHCb ϵ_{eff} is around 5%.

7 Hadron Identification

Figure 24a shows the momentum distribution of the pion with the highest momentum from $B_d \rightarrow \pi^+ \pi^-$ which is within the angular acceptance of LHCb. Similarly Fig. 24b shows the momentum distribution of kaons originating from the decay of the tagging B via the cascade $b \rightarrow c \rightarrow s$. Despite the fact that LHCb will operate with pp-interactions

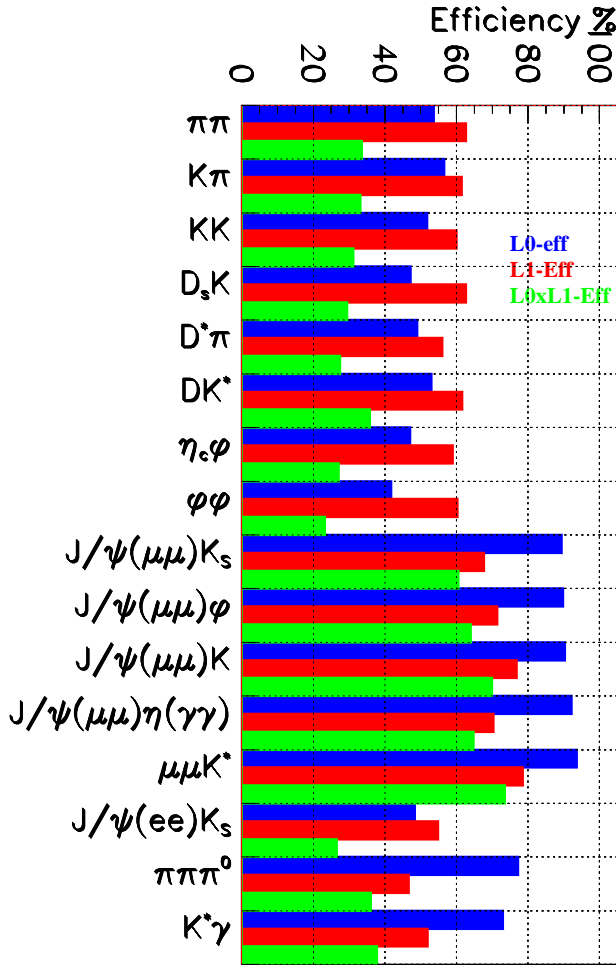


Figure 22. Efficiency of the first two trigger levels in LHCb for events which are accepted by the off-line reconstruction. For each channel the Level-0, Level-1 and combined efficiency is given.

at 14 TeV, the momentum of the tagging kaons which traverse the spectrometer starts around 1 GeV. LHCb is equipped with two RICH detectors [30, 19] to provide $\pi/K/p$ identification over a momentum range of 2 to 100 GeV/c. RICH1 is located before the magnet, and uses Aerogel and C_4F_{10} as radiators, which provide positive kaon identification above 2.0 GeV/c and 9.3 GeV/c respectively. RICH2 is sandwiched between the T3 tracker and the calorimeter, and its CF_4 gas threshold for kaons is 15.6 GeV/c. The photons are reflected and focused outside the LHCb acceptance by spherical mirrors, and the total area to cover with segmented photon detectors is 2.6 m². The typical segmentation required at the focal plane is 2.5 × 2.5 mm², and will be equipped with Pixel Hybrid Photon Detectors [31].

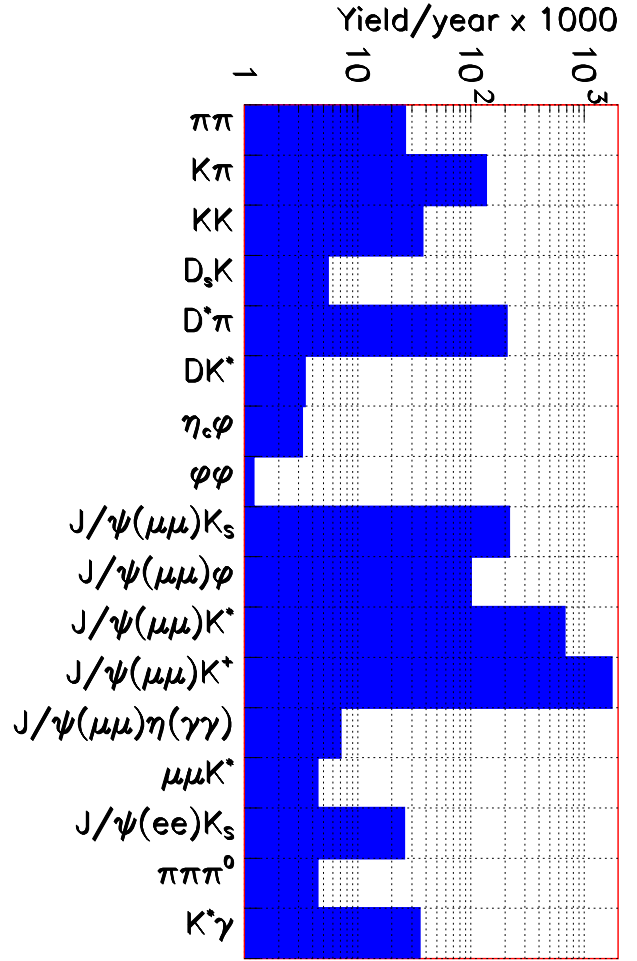


Figure 23. Annual event yields expected by LHCb for some representative channels.

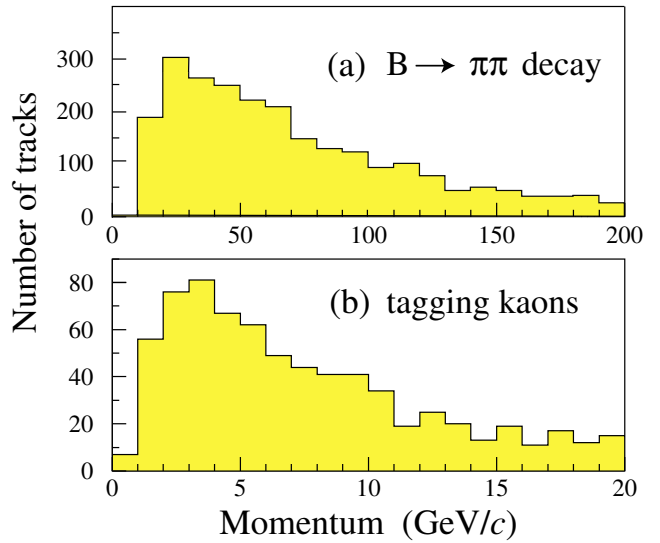


Figure 24. Momentum distribution of a) the pion with the highest momentum from $B_d \rightarrow \pi^+ \pi^-$ and b) tagging kaons in the LHCb acceptance.

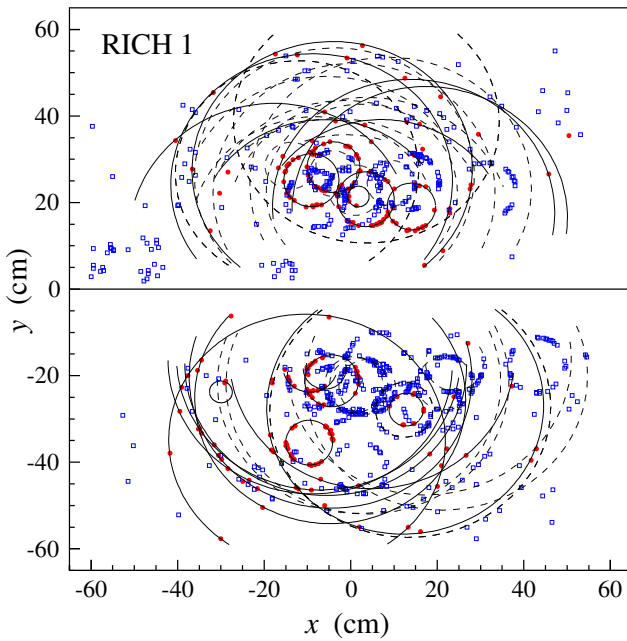


Figure 25. Event display of the RICH1 performance, showing the detected photons, the rings reconstructed for tracks which traverse the whole spectrometer (full lines), and the rings of local tracks (dashed lines).

Particle identification is performed by constructing a global likelihood including all tracks which have been reconstructed and the observed photon rings in the two RICH detectors. Fig. 25 shows an event display of a typical event, with the result of the reconstruction overlaid. The hadron identification performance of the two RICH detectors is illustrated in Fig. 26, which shows the invariant mass distribution of two oppositely charged pions with the RICH information taken into account. Neither ATLAS nor CMS are equipped with dedicated π/K separation detectors, and hence the signal from all the two-body decays of b-hadrons cannot be distinguished on an event by event basis. Fig. 27 shows the invariant $\pi^+\pi^-$ mass distribution of ATLAS, where the signal is dwarfed by background, coming mainly from $B_d \rightarrow K^+\pi^-$, $B_s \rightarrow \pi^+K^-$, $B_s \rightarrow K^+K^-$, and $\Lambda_b \rightarrow p\pi^-$ or pK^- .

8 Expected Asymmetry Sensitivities

The B-factories achieved a sensitivity of around 0.07 in $\sin(2\beta)$. All three LHC experiments expect to be able to get a precision of around 0.02 in this asymmetry after one year of running. Babar and Belle have measured $A_{\pi^+\pi^-}^{\text{mix}}$ and $A_{\pi^+\pi^-}^{\text{dir}}$ with precisions between 0.2 and 0.4 based on all their accumulated data so far. LHCb is expected to measure these asymmetries with a precision around 0.06 based on one year data taking. But more importantly, at the LHC one can access also the B_s decays. Combining the asymmetries measured in $B_d \rightarrow \pi^+\pi^-$ with its U-spin symmetric equivalent $B_s \rightarrow K^+K^-$, and assuming U-spin symmetry, allows LHCb to extract the angle γ with a precision of $4-6^\circ$, again based on the yield of one year. Time-dependent decay asymmetries in $B_s \rightarrow D_s^\mp K^\pm$ will yield $\sigma(\gamma) = 14-15^\circ$,

without theoretical assumptions. Another promising channel to determine γ without theoretical uncertainty is to study the time-integrated rates of $B_d \rightarrow D^0K^{*0}$, $B_d \rightarrow \bar{D}^0K^{*0}$ and $B_d \rightarrow D_{\text{CP}}^0K^{*0}$. Despite the small yield, i.e. only 600 $B_d \rightarrow D_{\text{CP}}^0K^{*0}$, $\sigma(\gamma) = 7-8^\circ$ is the expected precision, since these modes are flavour specific, and therefore do not require tagging. It must be noted that each of these three ways of measuring γ will be differently affected by physics beyond the Standard Model. The experiments have been designed to collect data for many years, hence allowing the angles of the CKM triangle to be determined with a precision of a few degrees.

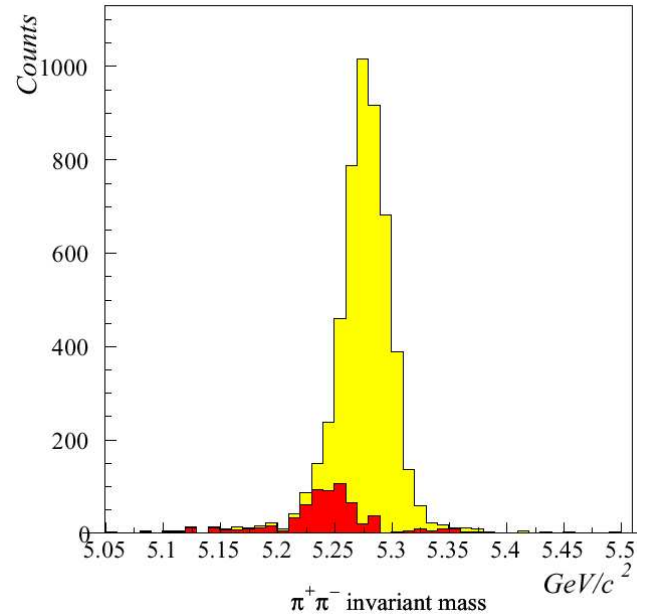


Figure 26. Invariant mass of $\pi^+\pi^-$ making use of the RICH information in LHCb. The remaining background is indicated with a dark shading.

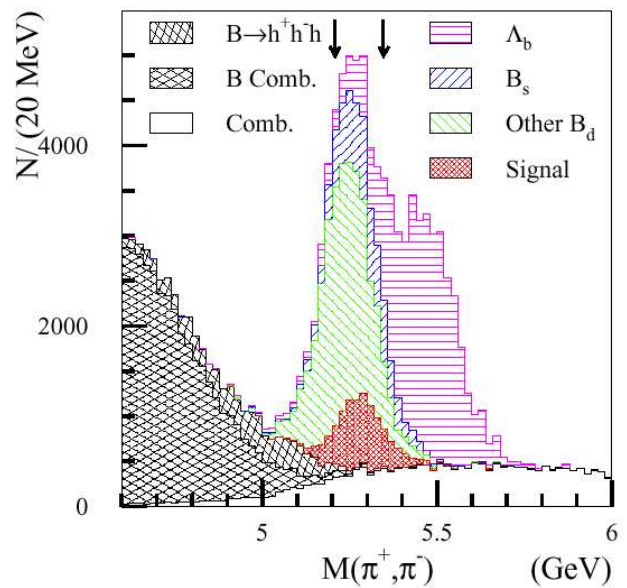


Figure 27. Invariant mass of $\pi^+\pi^-$ in ATLAS.

9 Conclusion

The first generation of CP violation experiments in the B-system, Belle and Babar at the B-factories, constrain the CKM matrix already considerably. The search for new physics beyond the Standard Model requires much larger statistics, combined with the study of other B-meson decays than those accessible at the B-factories, like B_s -decays. Three experiments are under construction to exploit the copious production of all B-flavours at the LHC: ATLAS, CMS and LHCb. While ATLAS and CMS have been designed to perform direct searches for Higgs and supersymmetry, LHCb is a dedicated experiment aimed at studying CP violation in the B-system. ATLAS and CMS are expected to contribute by measuring asymmetries mainly in channels with leptons in the final state for the first few years of LHC operation at luminosities an order of magnitude lower than the design luminosity. LHCb combines:

- a dedicated trigger system,
- excellent proper time resolution,
- good tracking,
- ability to identify charged and neutral hadrons, muons, electrons and photons,
- acceptable background rejection and
- adequate flavour tagging performance

in pursued of identifying new physics.

Acknowledgements

I would like to thank Dr. N. Tuning for providing the figures and numbers of the PYTHIA simulation, and Prof. T. Nakada for carefully reading the manuscript and many helpful suggestions.

References

- [1] M. Kobayashi and T. Maskawa, Prog. Theor. Phys. **49** (1973) 652.
N. Cabibbo, Phys. Rev. Lett. **10** (1963) 531.e
- [2] L. Wolfenstein, Phys. Rev. Lett. **51** (1983) 1945.
- [3] "The CKM matrix and the unitarity triangle", Workshop held at CERN, 13-16 February 2002, editors: M. Battaglia, A.J. Buras, P. Gambino and A. Stocchi. CERN-2003-002-corr, 10 October 2003.
- [4] M. Gronau and D. London, Phys. Rev. **D55**, 2845 (1997)
Y. Nir, hep-ph/0208080 v3 (2003)
- [5] A. Sakharov, JTEP Lett. **5**, 24 (1967)
- [6] From: <http://ckmfitter.in2p3.fr>
"A New Approach to a Global Fit of the CKM Matrix", H. Höcker, H. Lacker, S. Laplace and F. Le Diberder, Eur. Phys. J. **C21**, 225-259 (2001)
- [7] Belle Collaboration, A. Abashian et al., Nucl. Instr. Meth. **A479**, 117 (2002).
- [8] Babar collaboration, B. Aubert et al., Nucl. Instr. Meth. **A479**, 1 (2002)
- [9] K. Abe, et al.(Belle Collaboration), Phys. Rev. **D66**, (2002) 071102
- [10] B. Aubert, et al.(BaBar Collaboration), Phys. Rev. Lett. **89**, (2002) 201802
- [11] R. Fleischer and T. Mannel, hep-ph/0103121.
- [12] "Results on the CKM Angle $\phi_1(\beta)$ ", T.E. Browder, <http://conferences.fnal.gov/lp2003/program/index.html>.
- [13] <http://www.slac.stanford.edu/xorg/hfag/index.html>
- [14] K. Abe et al., Phys. Rev. **D67**, 03110(R) (2003)
- [15] B. Aubert et al., Phys. Rev. Lett. **89**, 281802 (2002), and updated numbers in "CKM Unitarity Angles $\alpha(\phi_2)$ and $\gamma(\phi_3)$ ", A. Jawahery, <http://conferences.fnal.gov/lp2003/program/index.html>.
- [16] "Interpreting CP Asymmetries in $B^0 \rightarrow \pi^+\pi^-$ decays", A. Höcker et al., LAL 2002-103.
- [17] R.D. Field, Phys. Rev. **D65**, 094006 (2002)
- [18] T. Sjöstrand and M. van Zijl, Phys. Rev. **D36**, 2019 (1987)
- [19] "LHCb Reoptimized Detector Design and Performance Technical Design Report", LHCb, CERN LHCC 2003-030.
- [20] P. Bartolini et al., LHCb/1999-028, contribution to the 1999 Workshop on Standard Model Physics (and more) at the LHC, CERN 2000-4, May 200.
- [21] ATLAS Detector and Physics Performance Technical Design Report, CERN/LHCC/99-14 and 99-15 (1999)
- [22] CMS Technical Proposal, CERN/LHCC 94-38, 1994.
- [23] L. Silvestris, Nucl. Phys. **B120**, 239 (2003)
- [24] E. Rose, Nucl. Phys. **B120**, 235 (2003)
- [25] U. Parzefall, Nucl. Phys. **B120**, 230 (2003)
- [26] S. Gadomski, Nucl. Phys. **B120**, 299 (2003)
- [27] J. Baines, Nucl. Phys. **B120**, 139 (2003)
- [28] CMS: The Trigger/DAQ Project, Technical Design Report, Vol II, CERN/LHCC 02-26 (2002).
- [29] LHCb Trigger System Technical Design Report, CERN/LHCC 2003-31 (2003).
- [30] LHCb RICH Technical Design Report, CERN/LHCC 2000-37 (2000).
- [31] M. Campbell et al., Nucl. Instr. Meth. **504**, 286 (2003)